Application of spectral statistics to surface defect detection

Hilda Deborah, Noël Richard, Jon Yngve Hardeberg

Hilda Deborah, Noël Richard, Jon Yngve Hardeberg, "Application of spectral statistics to surface defect detection," Proc. SPIE 11172, Fourteenth International Conference on Quality Control by Artificial Vision, 1117211 (16 July 2019); doi: 10.1117/12.2521714

SPIE.

Event: Fourteenth International Conference on Quality Control by Artificial Vision, 2019, Mulhouse, France

Application of Spectral Statistics to Surface Defect Detection

Hilda Deborah[1], Noël Richard[2], Jon Yngve Hardeberg[1]

[1]*Department of Computer Science, Norwegian University of Science and Technology, Norway*
[2]*Laboratory XLIM, JRU CNRS 7252, University of Poitiers, France*

ABSTRACT

The development of a spectral difference-based statistical processing of hyperspectral images is provided in this article. Kullback-Leibler pseudo-divergence function, which was specifically developed for the metrological processing of hyperspectral images, is used at the foundation of the statistics. As a demonstration of its use, the proposed statistics are used in visualising surface variability within a set of pigment patches. It is then further exploited to detect anomalies and deterioration that occur on the patches.

1. INTRODUCTION

Hyperspectral imaging has been used for quality control for, e.g., textile industry,[1,2] offset printing press,[3] and recycling plants.[4] This imaging technology offers a great accuracy thanks to its high spatial and spectral resolutions. Facing the lack of metrological solutions for the analysis of spectral measurements, in this work we propose several statistical tools that are based on a spectral difference space.

Despite data reduction or band selection techniques being the commonly used strategy in dealing with hyperspectral images,[5] data from all wavelengths are exploited in the proposed approach. With data reduction techniques, the acquired spectral accuracy gets removed before to analyse the data. Spectral differences between the different components of an observed surface, which is an important part of metrology, also cannot be preserved. The reason is because spectra are not vectors in the Euclidean space and, therefore, Euclidean metrics are not metrologically valid.[6] Furthermore, there is no valid addition and subtraction operations defined for reflectance spectra.[7] In order to develop metrological solutions, the proposed spectral statistics are based on the Kullback-Leibler pseudo-divergence function (KLPD),[8] which has been shown to respect all of the expected metrological constraints.[7]

In addition to providing the building blocks of the spectral difference-based spectral statistics, this work will also demonstrate their use in visualising and analysing the surface variability of a set of pigment patches. Specifically, the statistics will be used to detect anomalies or defects and discoloration in pigment patches.

2. DIFFERENCE-BASED STATISTICS FOR SPECTRAL DATA

2.1 Kullback-Leibler pseudo-divergence function

Kullback-Leibler pseudo-divergence (KLPD) function is a difference function specifically developed to enable a metrological processing of hyperspectral data,[8] assuming a contiguous wavelength sampling over a certain range. It measures the difference between two spectra S_1 and S_2 in terms of their shape ΔG and intensity ΔW:

$$\begin{aligned} d_{\mathrm{KLPD}}(S_1, S_2) &= \Delta G(S_1, S_2) + \Delta W(S_1, S_2) \\ \Delta G(S_1, S_2) &= k_1 \cdot d_{\mathrm{KL}}(\bar{S}_1, \bar{S}_2) + k_2 \cdot d_{\mathrm{KL}}(\bar{S}_2, \bar{S}_1) \\ \Delta W(S_1, S_2) &= (k_1 - k_2) \log\left(\frac{k_1}{k_2}\right) \end{aligned} \tag{1}$$

In computing ΔG, the two input spectra S_i will always be considered as probability density functions. This requires them to be normalised, therefore $\bar{S}_i$, in order to be used correctly within the Kullback-Leibler (KL) divergence function $d_{\mathrm{KL}}(\bar{S}_1, \bar{S}_2)$ as in (2). The normalisation procedure allows computing shape differences, while

Fourteenth International Conference on Quality Control by Artificial Vision, edited by Christophe Cudel, Stéphane Bazeille, Nicolas Verrier, Proc. of SPIE Vol. 11172, 1117211 · © 2019 SPIE · CCC code: 0277-786X/19/$21 · doi: 10.1117/12.2521714

neglecting the intensity information. For this reason, ΔW explicitly takes into account the intensity differences through the normalisation factors k_j of each spectrum $\bar{S}_j$. Details on the computation of KL divergence, a normalised spectrum, and its corresponding normalisation factor are as follows:

$$\begin{aligned} d_{\mathrm{KL}}(\bar{S}_1, \bar{S}_2) &= \int_{\lambda_{\min}}^{\lambda_{\max}} \bar{S}_1(\lambda) \cdot \log \frac{\bar{S}_1(\lambda)}{\bar{S}_2(\lambda)} \, d\lambda \\ \bar{S}_j = \left\{ \bar{s}_j(\lambda) = \frac{s_j(\lambda)}{k} \right\}, \; k_j &= \int_{\lambda_{\min}}^{\lambda_{\max}} s_j(\lambda) \, d\lambda \end{aligned} \tag{2}$$

Note that, strictly speaking, KLPD is not a distance function since it does not hold the property of triangular inequality. Additionally, the assessment of this spectral difference function has been carried out previously, both theoretically and through numerical experiments embedding metrological constraints.[7]

2.2 Histogram of spectral differences

A color image of a red pigment patch is shown in Figure 1a. Through visual observation, it can be seen that there are four different shades within the patch. The colors in each shade are not exactly the same. However, since their variations are relatively small, we can determine visually that each shade is relatively homogeneous in colors. This observation is also reflected in the spectral domain. Ten reflectance spectra are randomly selected from the patch and are shown in Figure 1b. First of all, it can be observed that all spectra have similar curves or shape, but vary in their intensity. Spectra belonging to the brighter red color will have bigger intensity, while those of the darker shade have smaller intensity. Secondly, there are also variations within the same shade, albeit small ones. The shape and intensity of spectra coming from the same shade are highly similar.

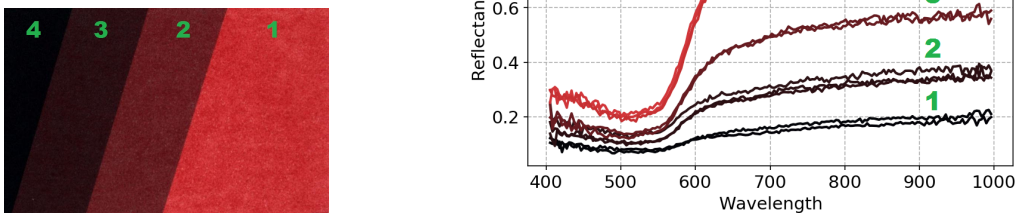

(a) Pigment OP-1 (b) Reflectance spectra

Figure 1: A red pigment patch and ten of its randomly selected reflectance spectra. The number annotations mark the pigment shade where the spectra comes from.

The previous observation made in the spectral domain was possible due to the low number of spectra being shown. But as the number of spectra increases, the discrimination we can make also decreases. Through the use of KLPD function, a spectrum can now be represented by a single difference value relative to any arbitrary spectral reference being used. This further allows the visualisation of a set of spectra $\mathcal{S}$ through a histogram of spectral differences (HSD) $\mathcal{D}_{\mathcal{S},S_{\mathrm{ref}}} = \{d_{\mathrm{KLPD}}(S_i, S_{\mathrm{ref}}), \forall S_i \in \mathcal{S}\}$. Using a theoretical equi-energetic white spectrum as reference $S_{\mathrm{ref}} = \{s_w(\lambda) = 1, \forall\lambda \subset [\lambda_{\min}, \lambda_{\max}]\}$, HSD of the pigment patch in Figure 1a are computed and shown in Figure 2a. In this visualisation, we can see four Gaussian-like distribution of pixels, representing the four shades of red that we can perceive in the pigment patch. Note that, in an HSD, the used spectral reference is always located at the origin. Thus, in the case of the illustrated HSD where a white spectrum is used as reference, the closest distribution to the origin is the brightest red while the farthest one corresponds to the darkest red.

The representation of a spectral set and, therefore, its distribution through KLPD space is not limited to one dimension. Since the difference function is composed of two components, i.e., shape and intensity, the histogram can be further decomposed into a two-dimensional one $\mathcal{D}_{\mathcal{S},S_{\mathrm{ref}}} = \{(\Delta G(S, S_{\mathrm{ref}}), \Delta W(S, S_{\mathrm{ref}})), \forall S \in \mathcal{S}\}$. The bidimensional histogram of spectral differences (BHSD) of the same pigment patch is shown in Figure 2b. It is

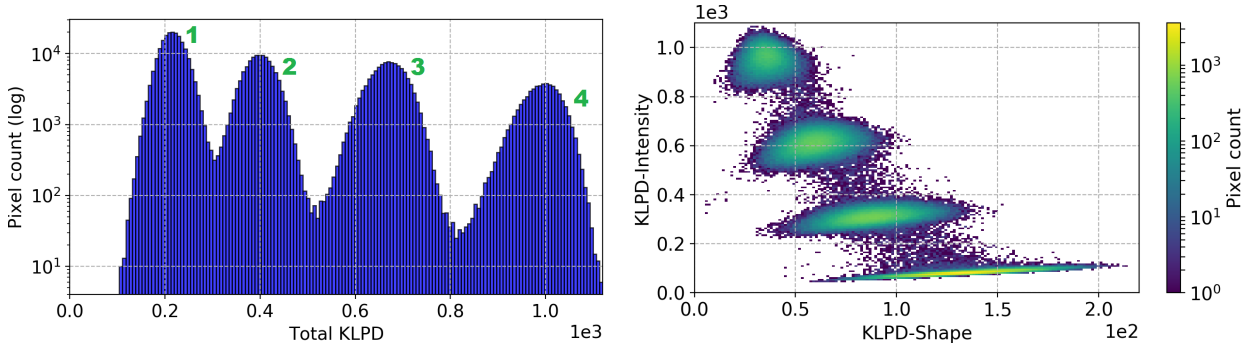

(a) (b)

Figure 2: Histogram of spectral differences (HSD) and bidimensional histogram of spectral differences (BHSD) of pigment patch in Figure 1a, computed relative to a theoretical equi-energetic white spectrum. Each numbered Gaussian-like distribution in the HSD corresponds to the same shade number in the pigment patch.

constructed relative to the same reference, i.e., theoretical equi-energetic white spectrum. As seen in the figure, pixels in the patch are still distributed within four main distributions corresponding to the pigment shades.

2.3 Statistical moments of a spectral difference set

Given a set of spectra or a spectral image, there exist no way of statistically modelling its pixel distribution directly from the n-dimensional acquisition or reflectance space. The task, however, can be translated into a spectral difference space as illustrated for a one-dimensional case in Figure 3. Given any arbitrary reference point x_{ref}, the probability density function of the pixels $P(x_i)$ is now observed relative to x_{ref}. Consequently, the average location is changed from μ to $\mu - x_{\text{ref}}$. In the higher dimensional spaces, the probability density function can be extended simply by means of a difference to the reference point $P(d(x_i, x_{\text{ref}}))$. Bear in mind that, by definition, a distance or divergence function is a positive measurement.

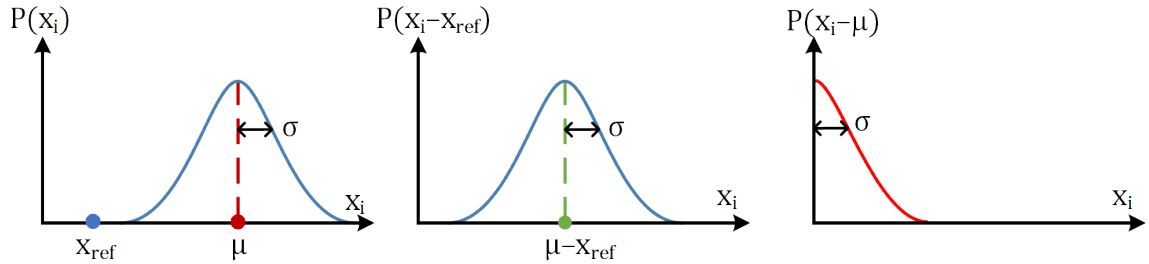

Figure 3: Illustration of the translation of univariate statistical moments of a one-dimensional probability density function $P(x_i)$ into a difference space relative to a reference point x_{ref} or to an average spectrum. Note that, by definition, the notion of difference always has positive values.

In the univariate domain, the first and second statistical moments are defined as follows:

$$\begin{array}{lllll} \text{Average} & \mu & = E[X] & = \sum_{x_i} x_i \cdot f(x_i) \\ \text{Variance} & Var(X) & = E[(X-\mu)^2] & = \sum_{x_i} (x_i - \mu)^2 \cdot f(x_i) \\ \text{Std. Deviation} & \sigma & = \sqrt{Var(X)} & \end{array} \tag{3}$$

To properly extend them to the spectral difference space, first, we have to carefully consider what is an average for spectral data. If a spectrum is regarded as a vector in the Euclidean space, the notion of average can be defined as the *spectrum of local average* $\overline{\mu}_{\mathcal{S}} = \{E[s(\lambda)], \forall\lambda \subset [\lambda_{\min}, \lambda_{\max}]\}$, where the average value is computed independently for each wavelength. This marginal processing of average spectrum, however, neglects the natural

interdependency between neighbouring wavelengths and almost always create a new false spectrum that does not exist in the initial set of spectra. The median spectrum $\widetilde{\mu}_{\mathcal{S}}$ is a good alternative to the average, since it is the closest spectrum to the theoretical average[9] and will always be a spectrum chosen from the set. To compute a median in the multivariate domain, typically, Vector Median Filters (VMF)[10] is used. However, it is computationally expensive and a more efficient alternative using a distance-based conditional ordering relation has been proposed.[11]

The second consideration to take in extending the univariate statistics in (3) to the spectral domain is the subtraction operation $(x_i - \mu)$. Direct subtraction has no sense neither in the physical nor optical domain. We are then forced to translate the purpose into the notion of difference. Finally, having defined the median $\widetilde{\mu}$ as alternative to the local average and extending the subtraction operation through the notion of difference, the standard deviation of a spectral difference set $\widetilde{\sigma}_{\mathcal{S}}$ can therefore be defined as follows:

$$\widetilde{\sigma}_{\mathcal{S}} = \sqrt{\sum_{S_i \in \mathcal{S}} \Big(d_{\mathrm{KLPD}}(S_i, \widetilde{\mu}_{\mathcal{S}})\Big)^2 f(S_i)} \tag{4}$$

As an example of the use of the statistics for spectral data, Figure 4a shows 200 randomly selected spectra from the brightest pigment shade in 1a and the median spectrum $\widetilde{\mu}$. Note that $\widetilde{\mu}$ is computed from all pixels of the shade and not only the 200 ones that are shown. Using this $\widetilde{\mu}$ as a reference, an HSD of the patch is obtained and shown in Figure 4b, along with the standard deviation $\widetilde{\sigma}$ computed for the set.

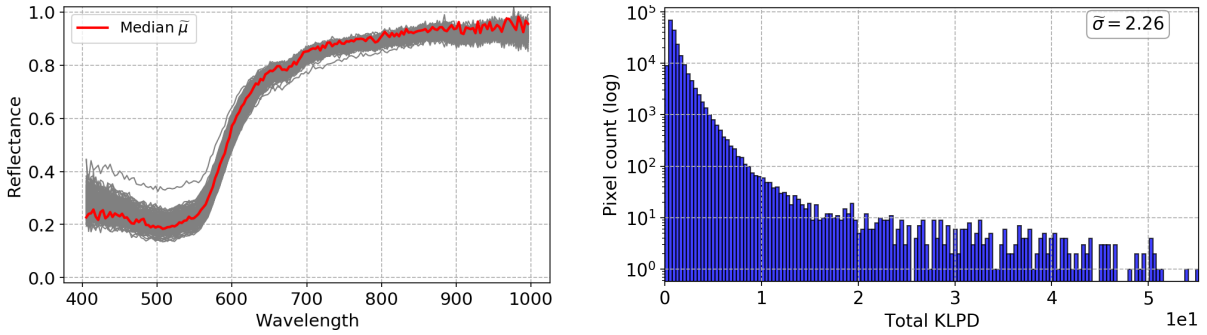

(a) Median spectrum $\widetilde{\mu}$ of shade-1

(b) HSD of shade-1 relative to $\widetilde{\mu}$

Figure 4: Median spectrum $\widetilde{\mu}$, HSD, and standard deviation $\widetilde{\sigma}$ of the set of spectra coming from shade-1 of the pigment patch shown in Figure 1a. Note that for observational purposes, (a) only shows 200 randomly selected spectra, plotted in gray color and (b) has a vertical axis shown in a log scale.

2.4 Structural statistical moments of a spectral difference set

The previous extension of statistical moments to the spectral domain was enabled by the representation of a spectral set $\mathcal{S}$ in an HSD. By further exploiting the decomposition of HSD to BHSD, a *spectral inner variance-covariance matrix*[12] $\widetilde{\Gamma}_{\mathcal{S}}$ can be defined as follows:

$$\widetilde{\Gamma}_{\mathcal{S}} = \begin{pmatrix} \alpha_{GG} & \alpha_{GW} \\ \alpha_{GW} & \alpha_{WW} \end{pmatrix} \text{ where } \begin{aligned} \alpha_{GG} &= \sum_{S_i \in \mathcal{S}} \Big(\Delta G(S_i, \widetilde{\mu}_{\mathcal{S}})\Big)^2 f(S_i) \\ \alpha_{WW} &= \sum_{S_i \in \mathcal{S}} \Big(\Delta W(S_i, \widetilde{\mu}_{\mathcal{S}})\Big)^2 f(S_i) \\ \alpha_{GW} &= \sum_{S_i \in \mathcal{S}} \Big(\Delta G(S_i, \widetilde{\mu}_{\mathcal{S}}) \cdot \Delta W(S_i, \widetilde{\mu}_{\mathcal{S}})\Big) f(S_i) \end{aligned} \tag{5}$$

Having defined $\widetilde{\Gamma}_{\mathcal{S}}$, Mahalanobis distance (MD) between any arbitrary spectrum S and a known spectral set $\mathcal{S}$ can be computed as written below. Note that this MD essentially computes distance in the normalised BHSD

space. The normalisation itself is against the variance-covariance matrix $\widetilde{\Gamma}$. Therefore, MD is analogous to the normalisation of an HSD relative to its standard deviation $\widetilde{\sigma}$.

$$d_M(S,\mathcal{S}) = \sqrt{d_{\mathrm{KLPD}}(S,\widetilde{\mu}_{\mathcal{S}})^T\ \widetilde{\Gamma}_{\mathcal{S}}^{-1}\ d_{\mathrm{KLPD}}(S,\widetilde{\mu}_{\mathcal{S}})} \tag{6}$$

3. DETECTION OF PRINTING ANOMALIES

An immediate application of the spectral statistics described in Section 2.3 is in detecting anomalies or outliers from hyperspectral images with stationary content, which will be provided in this section.

3.1 Dataset

Hyperspectral images coming from screen-printed pigment patches are used for this experiment, see Figure 5. The images vary in their spatial dimensions, typically around 850×550 pixels. Their spectral information covers 405.37–995.83 nm with 186 spectral bands. The shown color images were generated through color transformation involving CIE 1931 RGB color matching function (2° standard observer) and D65 illumination, mimicking how the human visual system perceives the patches under daylight.

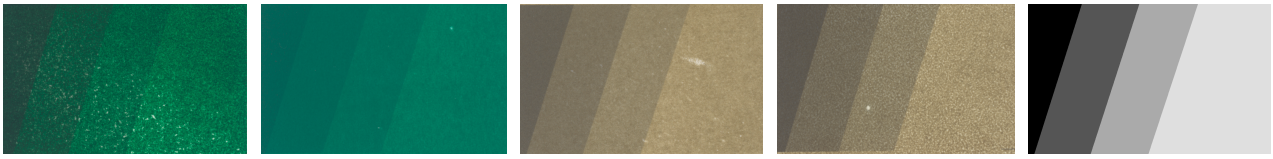

(a) GR-1 (b) GR-2 (c) GR-3 (d) OP-7 (e) Reference image

Figure 5: Pigment patches with printing defects and an example of reference image generated for GR-3.

Some spots can be observed on the pigment patches in Figure 5, which occur as a result of imperfect printing process. Knowing that there should be four relatively homogeneous color shades within each patch, a reference image segmenting the pigment shades are produced for each target. An example for pigment GR-3 can be observed in Figure 5e.

3.2 Experiment and results

Assuming a normal distribution, the empirical rule, or also known as 68-95-99.7 rule, will be used. This rule states that in a normal distribution, 99.7% of the population lie within three standard deviation from the the mean, or median in this case of spectral statistics. Therefore, anomalies are those pixels lying more than $3\widetilde{\sigma}$ away from the median $\widetilde{\mu}$. In order to use this threshold $t = 3\widetilde{\sigma}$, the statistics $\widetilde{\mu}$ and $\widetilde{\sigma}$ are obtained independently for each pigment shade. Pixels in the image are determined to belong to a shade according to the generated reference image.

To illustrate the steps of the experiment, the rightmost shade of pigment GR-3 will be used. Its original image is shown in Figure 6a, with the anomaly image next to it. This result is obtained by, first, computing spectral differences of the pixels relative to the median of the shade $\widetilde{\mu}$ using KLPD function. This further allows the visualisation in an HSD, as shown in Figure 6b, and also the $\widetilde{\sigma}$. Determination of anomalies is then carried out simply by drawing a threshold line at $3\widetilde{\sigma}$ in this HSD space. Anomalies are those located above the threshold. Finally, after carrying out the procedure for each individual shade and for all the four pigments, the final anomaly images for the used pigment patches are provided in Figure 7.

4. DETECTION OF PIGMENT DETERIORATION

Surface defects due to imperfect printing process is not the only problem that can disturb the surface of pigment patches. Pigments can deteriorate, either due to heat or other factors that happen during the storage. Figure 8a shows a color image of a pigment patch[1] that has deteriorated, generated mimicking its perception through

[1]Spatial characteristics of this patch is similar to those shown in Figure 5, while its spectral characteristics are identical.

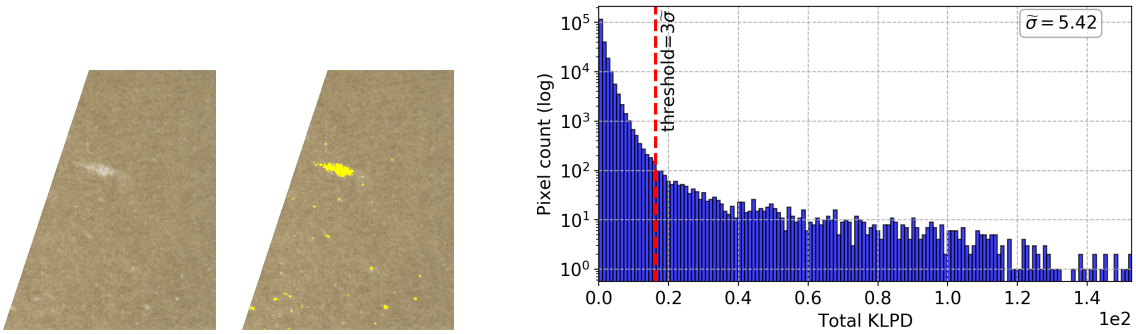

(a) (b)

Figure 6: (a) The rightmost shade of pigment GR-3 and the found anomalies marked by yellow pixels. (b) The anomalies are those pixels located above the threshold $3\widetilde{\sigma}$ in the shown HSD.

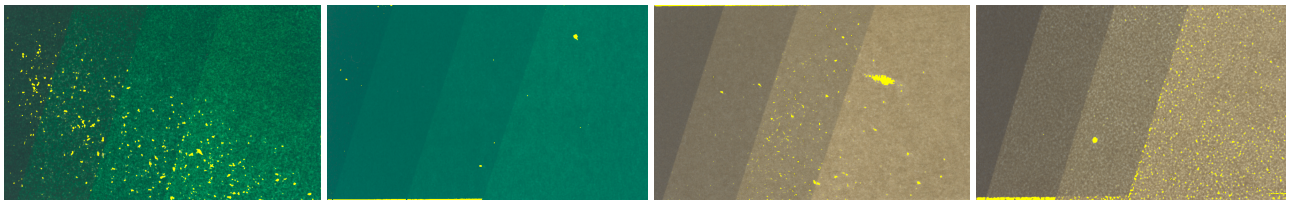

(a) GR-1 (b) GR-2 (c) GR-3 (d) OP-7

Figure 7: Final anomaly maps showing locations of defects on the surface of each pigment patches. The defects are those pixels colored in yellow.

the human visual system under daylight. Its rightmost shade has two main colors. One is a bright yellow, while the other one seems to be its darkened version. The deterioration becomes more evident in Figure 8b, which is generated by directly using the peak sensitivity of the hyperspectral sensor at 644.74, 552.19, and 466.01 nm as the RGB channels. Through this observation, it is evident that pixel distribution in the pigment shade is not unimodal.

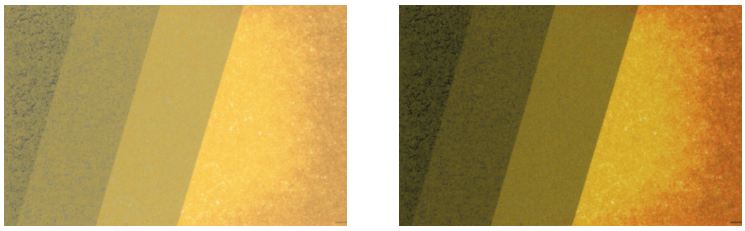

(a) (b)

Figure 8: Example of a pigment patch (OP-3) that has deteriorated. The first color image is generated the same way as those in Figure 5, mimicking the human visual system. The second color image is generated using the spectral bands at the sensor's peak sensitivity.

To analyse the content of a deteriorated pigment patch, observation can be carried out in the BHSD space. One is obtained for the rightmost shade of pigment OP-3 and is shown in Figure 9a, with variance-covariance matrix also provided. In this BHSD, two main directions of tails of the distribution can be observed, i.e., vertical and horizontal. However, this observation cannot be used to definitively say that the distribution is not unimodal. By further processing the BHSD into a Mahalanobis distance (MD) space, we can then start removing the outliers in the distribution. In this normalised space, and by assuming a normal distribution, the empirical rule is used again. Only pixels located within $3\widetilde{\Gamma}$ will be considered. Finally, Figure 9b is obtained, where two peaks can be observed from the distribution of pixels with MD lower than $3\widetilde{\Gamma}$. To fully automate the process, this final histogram of MD can be passed on to a unimodality test, e.g., dip test.[13]

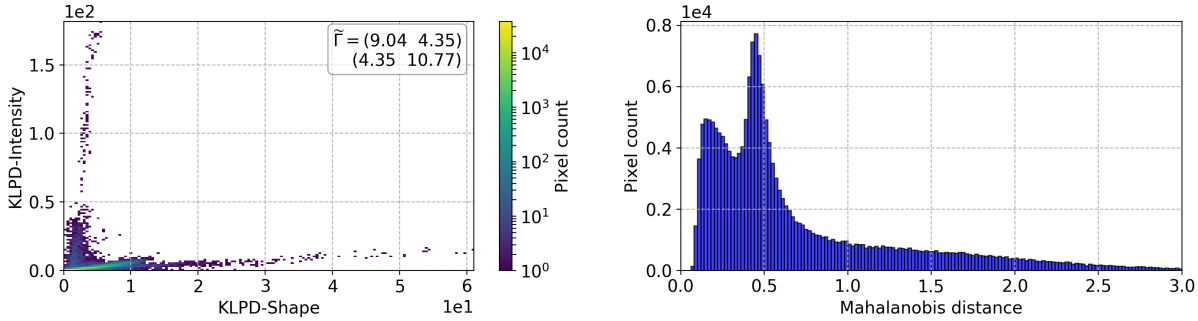

(a) (b)

Figure 9: (a) BHSD obtained for the rightmost shade of pigment OP-3, plotting all pixels within the shade. (b) Histogram of Mahalanobis distance obtained from normalising the BHSD against its variance-covariance matrix $\widetilde{\Gamma}$. This histogram only shows values below $3\widetilde{\Gamma}$.

5. CONCLUSION

Spectral difference-based statistics have been developed in this work. Its foundation is in the use of Kullback-Leibler pseudo-divergence (KLPD) function, which has been shown in a previous study to be satisfying the expected metrological properties. Through the use of this difference function, the task of statistically modelling the n-dimensional hyperspectral data can now be translated into the domain of one-dimensional spectral difference space. Due to the natural decomposition of KLPD into shape and intensity differences, the representation can be extended to a two-dimensional one, allowing more sensitivity to the spectral variability within an image.

The use of Mahalanobis distance as the immediate step from the definition of the statistical moments made it possible to use a normalised threshold. According to the empirical rule in statistics, 99.7% of the population in a normal distribution lie within three standard deviation from the median. Thus, this rule can be used to detect anomalies, which in this article was applied to screen-printed pigment patches. Pigment deterioration detection was also carried out in this study, assuming that the numbers of pixels corresponding to deteriorated pigments are quite significant. The determination of whether deterioration has happened was simply in being able to say that the distribution of pixels is not unimodal.

As a concluding remark, we have been able to develop the statistics for spectral data and use it for stationary content. The fact that we have been able to use the statistics in a straightforward manner and by simply using a normalised threshold, shows the potential of this approach. To continue this work, the statistical moments will be developed into a higher order ones, e.g., kurtosis and skewness, through the notion of directed distance.

ACKNOWLEDGMENT

This work is supported by FRIPRO FRINATEK Metrological Texture Analysis for Hyperspectral Images (projectnr. 274881) funded by the Research Council of Norway and French national projects ANR DigiPi and ERDF NUMERIC/e-Patrimoine.

REFERENCES

[1] Mirschel, G., Daikos, O., Scherzer, T., and Steckert, C., "Near-infrared chemical imaging used for in-line analysis of functional finishes on textiles," *Talanta* **188**, 91–98 (2018).

[2] Jin, X., Memon, H., Tian, W., Yin, Q., Zhan, X., and Zhu, C., "Spectral characterization and discrimination of synthetic fibers with near-infrared hyperspectral imaging system," *Appl. Opt.* **56**, 3570–3576 (Apr 2017).

[3] Mirschel, G., Daikos, O., Heymann, K., Scherzer, T., Genest, B., Sommerer, C., and Steckert, C., "In-line monitoring of the conversion in UV-cured printed layers by NIR spectroscopy in an offset printing press," *Prog. Org. Coat.* **77**(3), 719–724 (2014).

[4] Serranti, S., Gargiulo, A., and Bonifazi, G., "Hyperspectral imaging for process and quality control in recycling plants of polyolefin flakes," *J. Near Infrared Spec.* **20**(5), 573–581 (2012).

[5] Cao, X., Ji, Y., Wang, L., Ji, B., Jiao, L., and Han, J., "Fast hyperspectral band selection based on spatial feature extraction," *J. Real Time Image Process.* **15**, 555–564 (Oct 2018).

[6] Deborah, H., Richard, N., and Hardeberg, J. Y., "A comprehensive evaluation on spectral distance functions and metrics for hyperspectral image processing," *IEEE J. Sel. Topics Appl. Earth Observ. Remote Sens.* **8**(6), 3224–3234 (2015).

[7] Deborah, H., *Towards Spectral Mathematical Morphology*, phdthesis, Norwegian University of Science & Technology, University of Poitiers (Dec 2016).

[8] Richard, N., Helbert, D., Olivier, C., and Tamisier, M., "Pseudo-divergence and bidimensional histogram of spectral differences for hyperspectral image processing," *J. Imaging Sci. Technol.* **60**(5), 50402–1–13 (2016).

[9] Justusson, B. I., "Median filtering: Statistical properties," in [*Two-Dimensional Digital Signal Processing II: Transforms and Median Filters*], 161–196, Springer Berlin Heidelberg (1981).

[10] Astola, J., Haavisto, P., and Neuvo, Y., "Vector median filters," *Proc. IEEE* **78**(4), 678–689 (1990).

[11] Deborah, H., Richard, N., Hardeberg, J. Y., and Fernandez-Maloigne, C., "Assessment protocols and comparison of ordering relations for spectral image processing," *IEEE J. Sel. Topics Appl. Earth Observ. Remote Sens.* **11**(4), 1253–1265 (2018).

[12] Deborah, H., Richard, N., and Hardeberg, J. Y., "Application of spectral statistics to spectral texture discrimination," in [*Colour and Visual Computing Symposium (CVCS)*], 1–6 (Sep. 2018).

[13] Hartigan, J. A. and Hartigan, P. M., "The dip test of unimodality," *Ann. Statist.* **13**(1), 70–84 (1985).